Available online at www.sciencedirect.com
ScienceDirect
Journal of the European Ceramic Society 27 (2007) 3489–3496
www.elsevier.com/locate/jeurceramsoc

Evolution of elastic properties and microstructural changes versus temperature in bonding phases of alumina and alumina–magnesia refractory castables

Jean-Michel Auvray [a], Christian Gault *, Marc Huger

Groupe d'Etude des Matériaux Hétérogènes (GEMH), ENSCI, 47 à 73 Avenue Albert Thomas 87065 Limoges, France

Received 16 June 2006; received in revised form 18 January 2007; accepted 27 January 2007
Available online 20 April 2007

Abstract

The microstructural evolutions of high alumina refractory concretes, based on the systems $CaO–Al_2O_3$ and $CaO–Al_2O_3–MgO$, have been studied by the way of ultrasonic high temperature measurements. Since such a refractory concrete can be considered as a composite material with two constituents, a continuous matrix (so called bonding phase) and aggregates, investigations of matrices made of mixtures containing cement, reactive alumina and/or magnesia, constitute a preliminary study which is presented in this paper. The elastic behaviour of these matrices has been followed from room temperature to 1550 °C via a specific ultrasonic method. During the first thermal treatment, different changes of slope are observed in the curve $E = f(T)$. Between 200 °C and 400 °C, dehydration mechanisms involve a microstructural reorganisation correlated with a strong decrease of the elastic properties. At high temperature, the Young's modulus evolutions are associated with the expansive formations of CA_2 [b] and/or in-situ spinel at 1100 °C and then CA_6 (see endnote b) at 1450 °C, which directly depend on the CaO/Al_2O_3 and MgO/Al_2O_3 ratios in the mix. The forming of bond linkage between CA_6 and in-situ spinel grains in the matrix is believed to enhance the elastic properties at high temperature.

Keywords: Firing; Non-destructive evaluation; Mechanical properties; Spinels; Refractories

1. Introduction

Both alumina–spinel and alumina–magnesia castables are widely used in steel ladle linings, replacing high alumina bricks. In the future, the part of alumina–magnesia castables in the refractory market will probably progress taking into account their lower cost and their better high temperature performance, compared to synthetic spinel castables. For this system, we observe a high refractoriness and a better corrosion resistance than for Al_2O_3 castables.[1] During the first thermal treatment of the castable, the spinel $MgAl_2O_4$ is formed in the bonding phase by reaction between magnesia and alumina. Unfortunately, this reaction is associated with a sharp volume expansion of 3.7%[2] between 1200 °C and 1400 °C, which can damage the material in service. However, compared with alumina–spinel castables, the lifetime of the MgO materials can be significantly increased.[3,4] This could be attributed to a higher densification of the matrix at high temperature, thus reducing slag penetration and corrosion.[5] For Korgul et al., MgO contained in the castable is partially dissolved by the slag, leading to a high viscous MgO-rich less corrosive slag.[6,7] Additionally, the CaO of the slag reacts at high temperature with the Al_2O_3 of the castable to form CA_2 at 1200 °C, and CA_6 above 1400 °C. Furthermore, Criado and Estrada studied the dilatometric effects associated with the expansive formations of these calcium aluminates.[8] It is related in the literature that these high temperature resulting phases may interlock and link with other phases, thus improving the properties of the castable.[9] In particular, some authors attribute the enhancement of strength at high temperature in Al_2O_3–spinel castables to a strong interlocking bond between CA_6 and spinel grains in the matrix at high temperature.[10] Thus, during the first use of the refractory castable, it is advisable to control the multiple reactions between CaO, Al_2O_3, spinel or MgO which lead to evolutions of microstructure and mechanical properties.

* Corresponding author. Tel.: +33 5 55 45 22 35; fax: +33 5 55 79 09 98.
E-mail address: c_gault@ensci.fr (C. Gault).
[a] Present address: KERNEOS Aluminates Technologies, 95 rue du Montmurier, ZI Parc de Chesnes, 38291 Saint-Quentin Fallavier.
[b] Cement notation: $CaO=C$, $Al_2O_3=A$, $CaO–Al_2O_3=CA$, $CaO–2Al_2O_3=CA_2$, $CaO–6Al_2O_3=CA_6$, $MgO–Al_2O_3=MA$.

0955-2219/$ – see front matter © 2007 Elsevier Ltd. All rights reserved.
doi:10.1016/j.jeurceramsoc.2007.01.016

Such materials can be considered as composites with the bonding phase being the matrix and aggregates being reinforcement particles.[11] Properties of the concretes at high temperature are strongly dependent upon microstructural evolutions and reactions between constituents in the matrix. Therefore, it is fundamental to understand these mechanisms in order to predict the high temperature behaviour of the industrial refractory concrete. The work reported in this paper investigates correlations between microstructural changes and elastic properties of alumina and alumina–magnesia cementitious matrices during heat treatments. The evolutions versus temperature of the elastic properties of these compositions have been followed using an ultrasonic technique. The great sensitivity of Young's modulus to microstructural changes makes it a good mechanical parameter to characterise the behaviour of such materials at high temperature.

The matrices were constituted of a mix of the hydraulic cement and of the finest powders used for concrete fabrication (alumina, spinel or/and magnesia), conventionally having diameters lower than 100 μm. Above this arbitrary threshold value, particles become part of the aggregate phase of concretes.[11]

Two cement-bonded matrices are considered in this paper: a high-alumina composition termed MatA and an alumina–magnesia mixture termed MatAM. The first part of the paper deals with the identification of the effects on elasticity and thermal expansion of different phase changes, occurring from the dehydration process up to sintering at high temperature, in a pure cement phase (CEM). The behaviours of the two matrices are then investigated.

2. Experimental

2.1. Fabrication of materials

Some characteristics of the raw materials used for this work are listed in Table 1. High alumina cement (CA14M, $d_{50} = 11$ μm) contains mainly calcium mono and di-aluminates noted CA and CA_2, respectively, some alumina α-A and a minor phase $C_{12}A_7$ (see Table 2). The fine particles used as fillers are reactive alumina (CT3000SG and CL370C, $d_{50} = 0.5$–2 μm). Fine MgO powder ($d_{50} = 1$ μm) is a sintered seawater magnesia. Darvan 7S (0.05 wt.%, from Vanderbilt) was used as dispersant. The materials studied in this paper are to be used as matrices for two concretes, the compositions of which are given in Table 3.

Table 2
Wt.% compositions of mineralogical phases of CA14M cement

	Mineralogical phases			
Cement CA14M	A	CA	CA_2	$C_{12}A_7$
Wt.%	6	56	38	<1

Table 3
Compositions (wt.%) of the castables made with the two studied matrices: concrete A with MatA, concrete M with MatAM

Materials	Concrete A	Concrete M
Cement	5.50	5.50
Reactive alumina		
CT3000SG	3.80	2.60
CL370C	10.20	8.40
Tabular alumina		
45 μm	3.80	3.80
0–1 mm	28.80	15.70
0–3 mm	3.00	8.70
0–5 mm	27.00	32.40
1–2 mm	18.00	20.00
Magnesia	0.00	3.00
Water	5.00	5.50

A cementitious composition, referred as CEM, was first prepared by mixing 100 g of cement and 33 g of water, corresponding to a water/cement ratio of 0.33 (noted W/C = 0.33), typically used for cement characterisation. Then, a $CaO–Al_2O_3$ composition referred as MatA was prepared to simulate the matrix of the concrete A. This material consists in a mix of 79 wt.% of Al_2O_3 and 21 wt.% of cement cast with a W/C ratio of 0.91 (the same ratio as for castables). Finally, a $CaO–Al_2O_3–MgO$ matrix, referred as MatAM, was also prepared by mixing 70 wt.% of Al_2O_3, 21 wt.% of cement and 9 wt.% of MgO (W/C = 1) to simulate the matrix composition of the magnesia concrete M. Materials were cast in a Perrier mixer by dry-mixing powders for 1 min before adding water and dispersant by wet-mixing for 4 min. The mixed preparation was placed by vibration into a 160 mm × 40 mm × 40 mm silicon mould and wrapped in a plastic bag for a 48 h curing at room temperature. After casting at room temperature, the specimens undergo a thermal treatment which consists in heating at 110 °C for 48 h before characterisation.

Table 1
Chemical compositions and physical characteristics of raw materials

	Chemical analysis (wt.%)							Physical properties		Commercial reference
	CaO	Al_2O_3	Na_2O	SiO_2	Fe_2O_3	MgO	Cl	Specific surface area (m^2/g)	Bulk density	
Cement	27.00	72.00	0.25	0.30	0.15	0.20	0.00	1.66	3.04	CA14M[a]
Reactive alumina	0.02	99.80	0.08	0.03	0.02	0.09	0.00	3.00; 7.00	3.91	CL370C[a]; CT3000SG[a]
Magnesia	0.40	0.01	0.00	0.00	0.01	98.10	1.23	6.40	3.03	Ankermag B20[b]

[a] From Alcoa.
[b] From Magnifin.

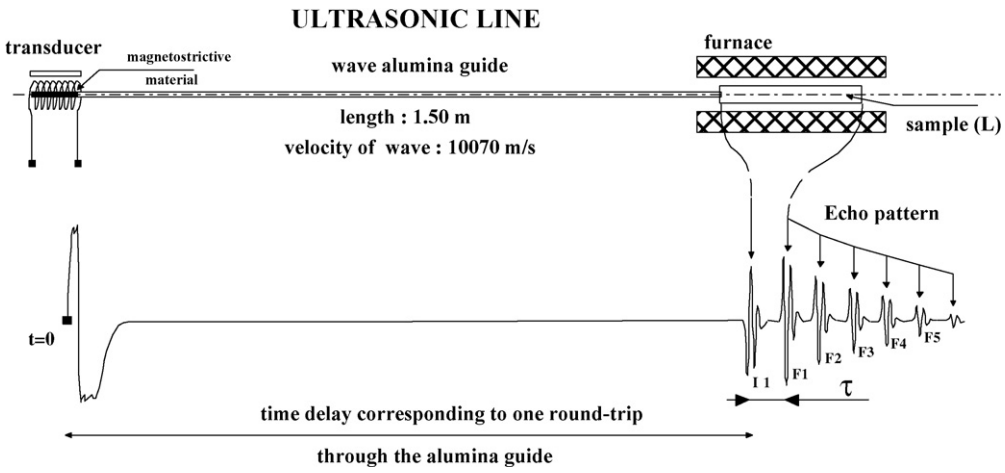

Fig. 1. Principle of ultrasonic Young's modulus measurements at high temperature.

2.2. Characterisation techniques

Measurements of the elastic modulus E of the specimens were made via a high temperature ultrasonic technique working in a long bar mode (lateral dimension of the propagation medium inferior to the wavelength), whose principle has been reported elsewhere.[12,13] This pulse-echo method uses ultrasonic compressional waves generated by a magnetostrictive transducer with frequencies ranging from 50 kHz to 110 kHz. The ultrasonic pulse is sent into the parallelepipedic sample through a refractory alumina wave guide. Fig. 1 presents the principle of the elastic modulus measurements. An electronic equipment (signal acquisition by a digital oscilloscope and a specific software package) automatically measures and records the time delay τ corresponding to one round-trip of the wave through the sample. Then, the Young's modulus E of the material is given by the following equation:

$$E = \rho\left(\frac{2L}{\tau}\right)^2 \quad (1)$$

where L and ρ are sample length and density, respectively.

The characteristics of the different parts of the ultrasonic line have been adapted to highly heterogeneous refractory concretes with large grains (up to 5 mm) and high porosity (up to 15%); this involves a low ultrasonic velocity and a high ultrasonic attenuation. The dimensions of samples and the wave frequency are 80 mm × 10 mm × 10 mm and 55 kHz, respectively. Experiments have been performed during a thermal treatment consisting in heating/cooling rates of 5 °C/min from room temperature to 1550 °C, with a dwell at 1550 °C for 2 h. The curves $E = f(T)$, presented in this paper, have been corrected for density variations and thermal expansion of the specimen as follows:

$$\frac{\Delta E(T)}{E_0} = \left(\frac{\tau_0}{\tau(T)}\right)^2 \left(1 - \frac{\Delta l(T)}{l_0}\right)\left(1 + \frac{\Delta m(T)}{m_0}\right) \quad (2)$$

where the suffix 0 is related to the values measured at room temperature, $\Delta m/m_0$ and $\Delta l/l_0$ are the relative variations of sample mass and length, respectively, obtained from TGA and thermal expansion measurements.

Bulk density and apparent porosity of specimens were measured by the Archimedes method in water (added with a wetting agent). Microstructures of sample fractures were examined by scanning electron microscopy (SEM). Thermal characterisations were carried out by differential thermal analysis (DTA) with a heating rate of 15 °C/min up to 1000 °C, in order to determine the successive thermal decompositions of the mineralogical cement phases. Thermal expansion measurements were performed in samples of dimensions 20 mm × 8 mm × 8 mm, using a high temperature dilatometer (ADAMEL DI24) at 5 °C/min from room temperature to 1500 °C. Mass losses have been monitored by thermogravimetric analysis (TGA), with an heating rate of 15 °C/min.

3. Results and discussion

3.1. Young's modulus evolutions versus temperature and thermal expansion of the cementitious paste CEM

Fig. 2 shows the Young's modulus evolutions and thermal expansion of CEM during an increase of temperature at a rate of 5 °C/min up to 1500 °C. Compared to thermally stable materials which exhibit regular variations of E and $\Delta l/l_0$ with temperature, the two curves show characteristic effects. Three domains can

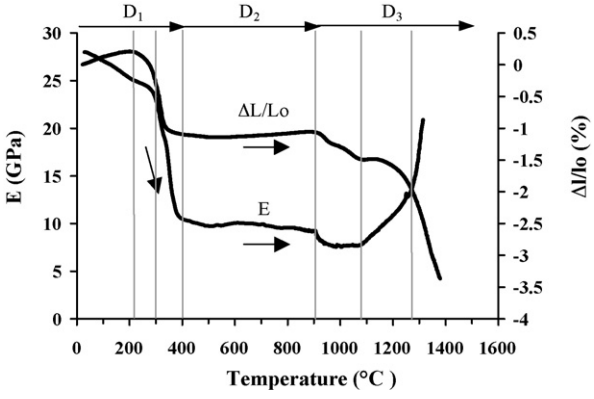

Fig. 2. Evolutions of thermal expansion and elastic modulus of CEM vs. temperature.

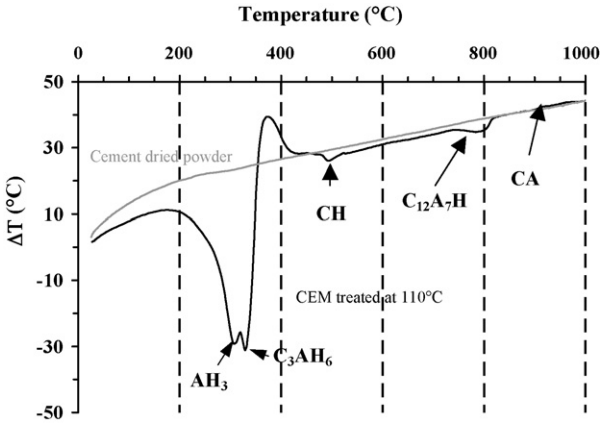

Fig. 3. Differential thermal analysis (DTA) of CEM treated at 110 °C.

be distinguished: D_1 from 20 °C to 400 °C; D_2 from 400 °C to 900 °C; D_3 above 900 °C.

3.1.1. Low temperature domain D_1

From room temperature to 200 °C, only regular thermal expansion and linear decrease of Young's modulus are observed. Above 200 °C, a shrinkage as well as a Young's modulus drop are observed. They have been attributed to dehydration mechanisms.

The expected phases in the starting material result from hydration of the anhydrous phases of the cement, after curing and heat treatment at 110 °C. Hydration mechanisms of a high alumina cement is well documented in the literature.[14–17] First, in normal conditions (room temperature), it is observed that metastable crystalline hydrates CAH_{10} and C_2AH_8 are jointly formed with an amorphous phase AH_3. Then, these metastable hydrates evolve to form stable hydrates C_3AH_6 and AH_3, as function of time and temperature. This phenomenon, commonly called "conversion" in literature,[18] can be accelerated by increasing temperature. It both involves a production of water and an important internal volume change (−37% from CAH_{10} to C_2AH_8/AH_3 and −53% from CAH_{10} to C_3AH_6/AH_3).[17] The consequence for the material is an increase of porosity and a weakening of mechanical properties. In the present work, the treatment at 110 °C was used to evaporate the excess free water and to fully convert the metastable phases into the stable hydrates C_3AH_6 and AH_3 which were the only crystalline phases detected by XRD after this step. Fig. 3 gives the result of a DTA experiment performed in CEM treated at 110 °C. Strong endothermic effects are observed in the range 200–400 °C, corresponding to the dehydration of the stable phases, which start at 210 °C for AH_3 and at 320 °C for C_3AH_6.

Table 4
Characteristics of anhydrous and hydrated phases of cement

Phase	Mass (%)		Molar mass (g/mol)	Density
	CaO	Al_2O_3		
C	100		56.08	3.30
$C_{12}A_7(H)$	48.6	51.4	1386.7	2.69
CA	35.4	64.6	158.04	2.98
CA_2	21.7	78.3	260	2.91
CA_6	8.4	91.6	667.84	3.38
A		100	101.96	3.98
CAH_{10}			338.04	1.72
C_2AH_8			358.12	1.95
C_3AH_6			378.20	2.52
AH_3			155.96	2.42

Table 5
Wt.% compositions of mineralogical phases of CEM treated at 110 °C

	Mineralogical phases				
	A	CA	CA_2	C_3AH_6	AH_3
Wt.%	4.90	6.40	31.20	31.50	26.00

During dehydration of cement, the release of water involves an important reorganisation of the microstructure. Based on the mineralogical composition of the cement and on phase densities (see Tables 4 and 5), the variation of the solid volume during dehydration can be estimated to −21% (see Table 6). Thus, the difference observed between this theoretical shrinkage and the experimental one, −4.5%, derived from the linear shrinkage, 1.5% measured in Fig. 2, denotes the formation of porosity (see Table 7). This can be responsible of the decrease of Young's modulus above 200 °C.

Moreover, there are other possible secondary causes for the E variations, such as the change in intrinsic elastic properties between hydrates and dehydrated phases, which could not be evaluated, and also the microcracking inside the microstructure involved by internal stresses due to shrinkage of grains during dehydration.

3.1.2. Intermediate temperature domain D_2

The thermal expansion and $E = f(T)$ curves do not exhibit any noticeable effect. The dehydrated material has very low Young's modulus (∼10 GPa). The small endothermic DTA peaks observed at 500 °C and 750 °C in Fig. 3 are related to the dehydration of CH and $C_{12}A_7H$, respectively.[19,20]

Table 6
Variation of the solid volumes of the cementitious phases before and after dehydration

	Phases (before, 110 °C)			Phases (after, 400 °C)				
	$\{A + CA + CA_2\}$	C_3AH_6	AH_3	$\{A + CA + CA_2\}$	$C_{12}A_7H$	CH	A	(H)
Mass (wt.%)	42.50	31.50	26	42.50	16.75	7.95	17	15.8
Solid volume (cm^3)	14.10	12.50	10.75	14.10	7.5	3.55	4.30	
Total solid volume (cm^3)	37.35			29.42 (−21% between 110 °C and 400 °C)				

Table 7
Characteristics of CEM before and after dehydration

	Before (110 °C)	After (400 °C)
Density/porosity (%)	1.91/24.5	1.70/46.7

3.1.3. High temperature domain D_3

Thermal decomposition of CH and $C_{12}A_7H$ produces C and $C_{12}A_7$. Between 900 °C and 1000 °C, CA is recrystallised by reaction between these phases and A, as it has been observed by XRD analysis. It involves a slight shrinkage (Fig. 2) mainly attributed to the difference of volume of solid phases formed according to equation:

$$C_{12}A_7 + 5A \rightarrow 12CA \quad (\Delta V/V = -1.14\%) \tag{3}$$

This reaction results in a change of microstructure associated with a decrease of elastic properties of the cementitious paste.

Between 1100 °C and 1200 °C, CA_2 is formed by reaction between CA and A:

$$CA + A \rightarrow CA_2 \quad (\Delta V/V = +13.6\%) \tag{4}$$

It results in a volume expansion of the material which opposes the shrinkage due to sintering as observed in Fig. 2. This expansive formation of CA_2 coincides with an increase of Young's modulus. A partial resorption of porosity and a reinforcement of the grain–grain contacts due to the CA_2 formation, in parallel with the beginning of sintering, can explain this stiffness increase. According to the assumed mineralogical composition of cement at 1000 °C (see Table 8), the amount of free Al_2O_3 in the material is not sufficient to form CA_6 by reaction between CA_2 and A:

$$CA_2 + 4A \rightarrow CA_6 \quad (\Delta V/V = +3.01\%) \tag{5}$$

Therefore, no additional expansion is observed above 1300 °C and the material exhibits a strong shrinkage attributed to sintering which involves also a large increase of Young's modulus.

3.2. Young's modulus evolutions and thermal expansion of MatA versus temperature

The different interactions occurring between cement and alumina in a $CaO–Al_2O_3$ matrix and their consequences on elastic properties are investigated in this section. The evolutions of thermal expansion and elastic modulus are shown in Fig. 4 as function of temperature.

The dehydration process results in similar effects to those previously observed for CEM, but with a lower amplitude, because cement is not the unique constituent of the matrix. For the same reason, the crystallisation of CA at 900 °C has only a very slight effect on the elasticity and on the thermal expansion. From 1100 °C to 1250 °C, the formation of CA_2 by reaction between CA and A involves a small expansion of the specimen. However, a difference has been observed between this experimental value and the value calculated from the mineralogical composition and density of the present phases (A, CA and CA_2), which was found higher (see Table 9). This difference can be explained by a partial resorption of porosity due to the expansion of CA_2. It is confirmed by a significant increase of Young's modulus. Micrograph of a fracture of the material fired at 1300 °C (see Fig. 5a) shows CA_2 globular crystals that give a cohesive microstructure after sintering.

Table 8
Wt.% compositions and solid volumes of CEM before and after formation of CA_2

	Phases (before, 1000 °C)			Phases (after, 1250 °C)		
	A	CA	CA_2	A	CA	CA_2
Wt.%	6	56	38	0	46.7	53.3
Solid volume (cm^3)	4.5	56.5	39	0	46	54

Table 9
Wt.% compositions and solid volumes of the MatA as function of temperature

	Phases					
	A	CA	CA_2	CA_6		
Mass (wt.%) at						
1000 °C	80.5	15	4.5	0		
1250 °C	71	0	29	0		
1550 °C	25.5	0	0	74.5		
					$\Delta V/V$ (%)	
					Theoretical	Experimental
Solid volume (cm^3) at						
1000 °C	75.5	18.7	5.8	0		
1250 °C	64	0	36	0	+3.7	+0.6
1550 °C	22.5	0	0	77.5	+2.3	>1.2

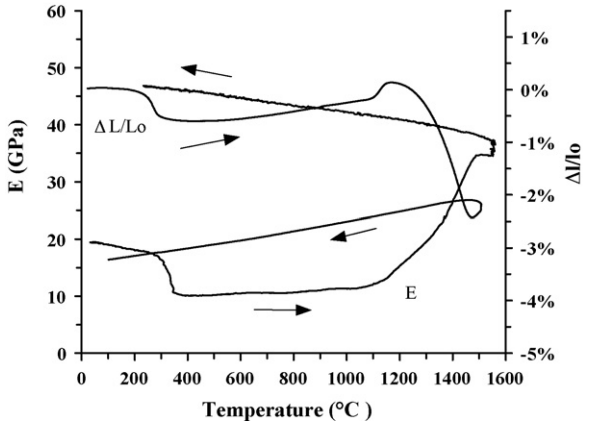

Fig. 4. Evolutions of thermal expansion and elastic modulus of MatA vs. temperature.

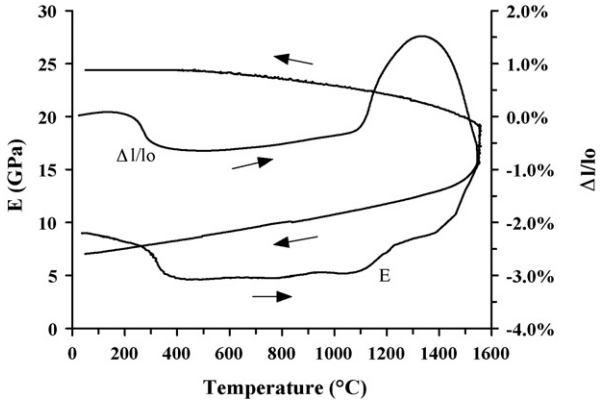

Fig. 6. Evolutions of thermal expansion and elastic modulus of MatAM vs. temperature.

At higher temperature, the densification of the matrix involves an important and regular increase of modulus due to sintering.

The main differences between the cement and the matrix composition are expected to occur at high temperature (>900 °C) with the formations of CA_2 and CA_6 which are favoured by an important amount of alumina. At 1450 °C, CA_2 reacts with A to form CA_6, according to Eq. (5), which is associated to a volume expansion of the material. The theoretical value of this expansion was calculated (see Table 9), according to the expected variation of the solid volume of the phases.[21] It appears to be lower than the experimental one (because of the difficulty to dissociate this expansion and the shrinkage due to sintering that occurs simultaneously). The hexagonal morphology of CA_6 grains and their anisotropic growth into platelet shape can result in an increase of porosity in this temperature range, which could explain this. It is confirmed by the microstructure observed in Fig. 5b after thermal treatment at 1550 °C/2 h, which clearly shows the porous random tangle of hexagonal platelets of CA_6. As a consequence, the previous regular modulus increase of the material is stopped when the formation of CA_6 occurs at 1450 °C.

3.3. Young's modulus evolutions and thermal expansion of MatAM versus temperature

The material studied in this section is based on the same composition as the $CaO–Al_2O_3$ matrix, but with a partial substitution of reactive alumina by magnesia. The purpose was to examine the effects of the in-situ formation of spinel on the mechanical properties. Fig. 6 shows the dilatometric and elastic behaviours of the material as a function of temperature. Note that the microstructural effects observed at low temperature (<1000 °C) are similar to those observed for MatA, explained by the dehydration process. Then, we will only focus on evolutions at high temperature (>1000 °C).

From 1050 °C to 1200 °C, the material exhibits a high volume expansion correlated to the cumulated formations of CA_2 and spinel $MgAl_2O_4$ by reaction between CA, A and MgO. The expected value of the expansion on the basis of the mineralogical composition was found to be close to the experimental one (see Table 10). In this case, in contrast to MatA, the resorption of porosity associated with the expansive formations of these phases is very low. Therefore, no significant variation of apparent porosity was observed by the Archimedes method for a specimen treated at 1200 °C/2 h. Similar results are related in

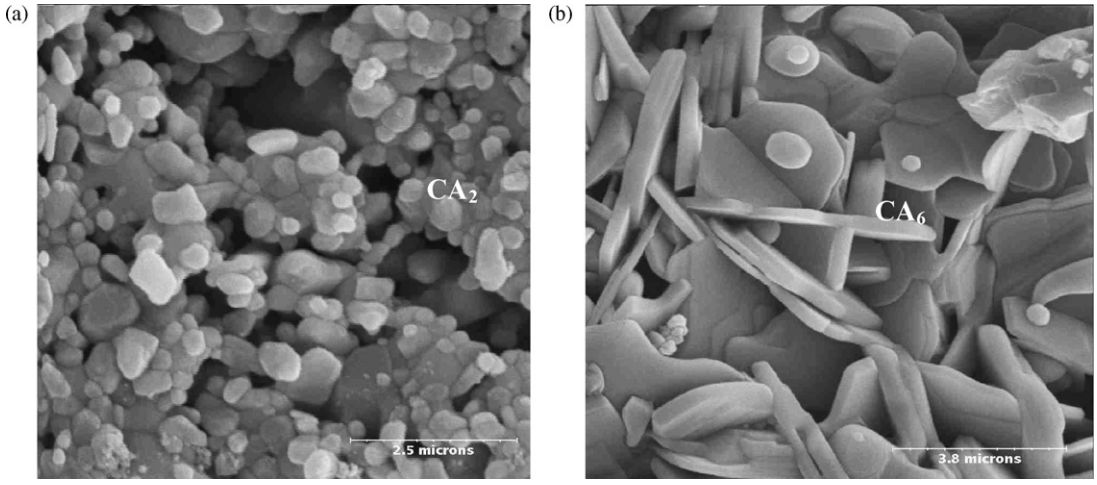

Fig. 5. SEM pictures of sample fractures of MatA fired at 1300 °C (a) and 1550 °C/2 h (b).

Table 10
Wt.% compositions and solid volumes of MatAM before and after formation of CA_2 and spinel

	Phases (before, 1000 °C)				Phases (after, 1300 °C)			
	A	CA	CA_2	MgO	A	CA	CA_2	MA
Wt.%	71.5	15	4.5	9	44	0	29	26.5
Solid volume (cm^3)	18	5	1.55	2.5	11	0	10	7.1

the literature.[22] At the same time, the Young's modulus versus temperature curve exhibits an increase of the slope attributed to the strengthening of the microstructure by improvement of grain–grain contacts and bonding between spinel and cement phases.

From 1200 °C to 1400 °C, a lessening of the increase in modulus is observed, in contrast to MatA. The presence of micropores associated with in-situ formation of spinel could act against sintering. Furthermore, the reactions associated to CA_2 and spinel formations involve a strong decrease of the quantity of free reactive alumina favourable to sintering.

At higher temperature, a regular increase of Young's modulus is observed which continues during the dwell at 1550 °C in contrast to what is observed for MatA. It shows that, in this case, the expansive formation of CA_6 at about 1450 °C does not involve a reduction in the curve of modulus. This can be explained by enhanced mechanisms of densification:

- sintering promoted by the presence of a viscous phase coming from impurities in the magnesia (in particular, CaO and Cl),
- filling by the CA_6 grains of the micropores induced by the in-situ formation of spinel,[22]
- alumina bridges between the spinel and CA_6, which would involve strong ceramic bonds, as shown by a micrography of the material fired at 1550 °C for 2 h (see Fig. 7).

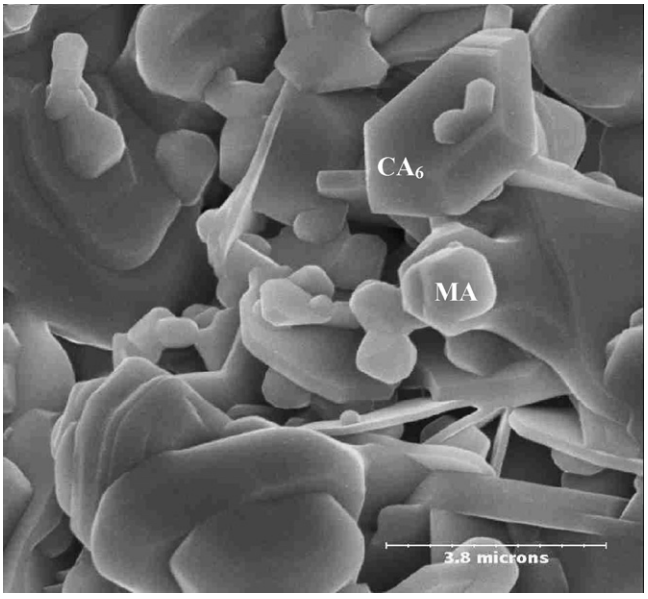

Fig. 7. SEM picture of a sample fracture of MatAM fired at 1550 °C/2 h.

Finally, XRD analysis confirms that the thermal treatment consisting in a firing at 1550 °C for 2 h is sufficient to obtain a complete formation of in-situ spinel and CA_6, and EDS patterns allowed the determination of the Al_2O_3 content in spinel. It was found to be around 76 wt.%, close to the stoichiometric composition and in agreement with results obtained by Ko et al. for similar materials.[23]

4. Conclusion

Microstructural evolutions and all phase changes occurring in cement–alumina and cement–alumina–magnesia matrices for the fabrication of refractory castables, have been characterised by ultrasonic measurements at high temperature.

For the two materials, between 150 °C and 400 °C, the dehydration process involves a volume shrinkage in parallel with a strong decrease of elastic modulus attributed to an increase of porosity.

It was found that the main difference between the behaviours of the two types of matrices occurs at high temperature during the in-situ formation of spinel in the case of the CaO–Al_2O_2–MgO matrix. From 1100 °C to 1250 °C, expansive formations of CA_2 and/or in-situ spinel coincide with a significant increase of Young's modulus. This effect drastically depends on the CaO/Al_2O_3 and MgO/Al_2O_3 ratios. At 1450 °C, the reduction in the slope of the Young's modulus versus temperature curve is attributed to the increase of porosity due to an anisotropic growth of CA_6 grains. This effect is lower for the MgO castable for which the densification of the matrix is the main mechanism in this temperature range. Moreover, for the magnesia used in this study, the presence of impurities can involve a viscous phase at high temperature, favourable to sintering. Microscopic observation of the MgO material heated at 1550 °C for 2 h reveals CA_6 crystals which grow out of the spinel grains in the bonding matrix of the castable. Bonding between the CA_6 and in-situ spinel grains is believed to be responsible for enhancement of the elastic properties at high temperature.

All these results obtained for the matrices will be used to interpret microstructural changes and mechanical evolutions at high temperature in castables.

Acknowledgement

The authors would like to express their gratitude towards the Vesuvius Company and the Council of Limousin Region for financial support of the present work.

References

1. Ko, Y. C., Effect of compositional variables on the properties of alumina-magnesia castables. *Interceram*, 2000, **49**(5), 316–325.
2. De Aza, A. H., Pena, P. and Iglesias, J. E., The system Al_2O_3–MgO–CaO Part II: relationship in the subsystem Al_2O_3–$MgAl_2O_4$–$CaAl_4O_7$. *J. Am. Ceram. Soc.*, 2000, **83**(4), 919–927.
3. Mori, J., Watanabe, N., Yoshimura, M., Oguchi, Y., Kawakami, T. and Matsuo, A., Material design of monolithic refractories for steel ladle. *Bull. Am. Ceram. Soc.*, 1990, **69**, 1172–1176.
4. Kobayashi, M., Kataoka, K., Sakamoto, Y. and Kifune, I., Use of alumina-magnesia castables in steel ladle sidewalls. *Taikabutsu Overseas*, 1997, **17**(3), 39–44.
5. Nanba, M., Kaneshige, T., Hamazaki, Y., Nishio, H. and Ebizawa, I., Thermal characteristics of castables for teeming ladle. *Taikabutsu Overseas*, 1996, **16**(3), 17–21.
6. Korgul, P., Wilson, D. R. and Lee, W. E., Microstructural analysis of corroded alumina-spinel castable refractories. *J. Eur. Ceram. Soc.*, 1997, **17**, 77–84.
7. Fuhrer, M., Hey, A. and Lee, W. E., Microstructural evolution in self-forming spinel/calcium aluminate-bonded castable refractories. *J. Eur. Ceram. Soc.*, 1998, **18**(7), 813–820.
8. Criado, E., Estrada, D. A. and De Aza, S., Dilatometric study of the formation of CA_2 and CA6 in cements and refractory concretes. *Bull. Sp. Ceram. Glass Soc.*, 1976, **15**(5), 319–321.
9. Vance, M. W., Kriechbaum, G. W., Henrichsen, R. A., MacZura, G., Moody, K. J. and Munding, S., Influence of spinel additives on high-alumina/spinel castables. *Bull. Am. Ceram. Soc.*, 1994, **73**, 70–74.
10. Ko, Y. C. and Chan, C. F., Effect of spinel content on hot strength of alumina-spinel castables in the temperature range 1000–1500 °C. *J. Eur. Ceram. Soc.*, 1999, **19**, 2633–2639.
11. Auvray, J. M., Elaboration et caractérisation à haute température de bétons réfractaire à base d'alumine et de spinelle, Thesis, Limoges University, France, 2003.
12. Gault, C., Ultrasonic non destructive evaluation of microstructural changes and degradation of ceramics at high temperature. In *Am. Mater. Res. Symp. Proc.*, ed. J. Holbrook and J. Bussiere. 1989, pp. 142, 263–274.
13. Huger, M., Fargeot, D. and Gault, C., High-temperature measurement of ultrasonic wave velocity in refractory materials. *High Temperatures-High Pressures*, 2002, **34**, 193–201.
14. Capmas, A. and Ménétrier-Sorrentino, D., The effect of temperature on the hydration of calcium aluminate cement. *Unitecr'89*, 1989, **2**, 1157–1170.
15. Cottin, B., The first reactions in cement hydration. In *Proceedings of the International RILEM Workshop on Hydration and Setting of Cements*, ed. A. Nonat and J. C. Mutin. Dijon, France, 1991.
16. Jung, M., Hydraulic properties of high-alumina cements. In *International Symposium on Refractory Concretes*, 1971.
17. Kopanda, J. E. and Maczura, G., Production processes, properties, and applications for calcium aluminate cements. In *Alumina, Science and Technology Handbook Chemicals*, ed. L. D. Hart. J. Am. Ceram. Soc., Westerville, 1990, pp. 171–183.
18. Mehta, P. K. and Lesnikoff, G., Conversion of CaO–Al_2O_3 $10H_2O$ to 3CaO–$Al_2O_3$6H_2O. *J. Am. Ceram. Soc.*, 1971, **54**(4), 210–212.
19. Kuzel, H. J., Uber die orientierte entwässerung von tricalciumaluminathydrat $3CaOAl_2O_3$. $6H_2O$. *Neues Jahrbuch für Mineralogie Monatshefe*, 1969, 397–403.
20. Ball, M. C., The thermal dehydroxylation of C_3AH_6. *Cem. Conc. Res.*, 1976, **6**, 419–420.
21. Givan, G. V., Hart, L. D., Heilich, R. P. and MacZura, G., Curing and firing high purity calcium aluminate-bonded tabular alumina castables. *Ceram. Bull.*, 1975, **54**(8), 710–713.
22. Naaby, H., Abildgarrd, O., Stallmann, G., Wohrmeyer, C. and Meidell, J., *Refractory wear mechanism and influence on metallurgy and steel quality as result of the conversion to endless lining at Det Danske Stalvalsevaerk*. Stahl und Eisen Special, Verlag Stahleisen GmbH, Düsseldorf, 1994, pp. 198–204.
23. Ko, Y. C., Influence of the characteristics of spinels on the slag resistance of Al_2O_3–MgO and Al_2O_3–spinel castables. *J. Am. Ceram. Soc.*, 2000, **83**(9), 2333–2335.